HHS Public Access

Author manuscript

J Control Release. Author manuscript; available in PMC 2019 May 10.

Published in final edited form as:

J Control Release. 2018 May 10; 277: 89–101. doi:10.1016/j.jconrel.2018.03.006.

Transferrin-targeted, resveratrol-loaded liposomes for the treatment of glioblastoma

Aditi Jhaveri[*], **Pranali Deshpande**[*], **Bhushan Pattni**[*], and **Vladimir Torchilin**[*,1]

[*]Center for Pharmaceutical Biotechnology and Nanomedicine, Department of Pharmaceutical Sciences Northeastern University Boston MA 02115

Abstract

Glioblastomas (GBMs) are highly aggressive brain tumors with a very grim prognosis even after multi-modal therapeutic regimens. Conventional chemotherapeutic agents frequently lead to drug resistance and result in severe toxicities to non-cancerous tissues. Resveratrol (RES), a natural polyphenol with pleiotropic health benefits, has proven chemopreventive effects in all the stages of cancer including initiation, promotion and progression. However the poor physico-chemical properties of RES severely limit its use as a free drug. In this study, RES was loaded into PEGylated liposomes (RES-L) to counter its drawbacks as a free drug. Since transferrin receptors (TfRs) are up-regulated in GBM, the liposome surface was modified with transferrin moieties (Tf-RES-L) to make them cancer cell-specific. The liposomal nanomedicines developed in this project were aimed at enhancing the physico-chemical properties of RES and exploiting the passive and active targeting capabilities of liposomes to effectively treat GBM.

The RES-L were stable, had a good drug-loading capacity, prolonged drug-release *in vitro* and were easily scalable. Flow cytometry and confocal microscopy were used to study the association with, and internalization of, Tf-L into U-87 MG cells. The Tf-RES-Ls were significantly more cytotoxic and induced higher levels of apoptosis accompanied by activation of caspases 3/7 in GBM cells when compared to free RES or RES-L. The ability of RES to arrest cells in the S-phase of the cell cycle, and selectively induce production of reactive oxygen species in cancer cells were probably responsible for its cytotoxic effects. The therapeutic efficacy of RES formulations was evaluated in a subcutaneous xenograft mouse model of GBM. A tumor growth inhibition study and a modified survival study showed that Tf-RES-Ls were more effective than other treatments in their ability to inhibit tumor growth and improve survival in mice. Overall, the liposomal nanomedicines of RES developed in this project exhibited favorable *in vitro* and *in vivo* efficacies, which warrant their further investigation for the treatment of GBMs.

Graphical abstract

Corresponding Author address: Center for Pharmaceutical Biotechnology and Nanomedicine, Northeastern University, 360 Huntington Ave, 140 The Fenway, Room 216, Boston, MA 02115, USA. v.torchilin@neu.edu; Tel: 617-373-3206; Fax 617-373-7509.

Conflicts of interest: None

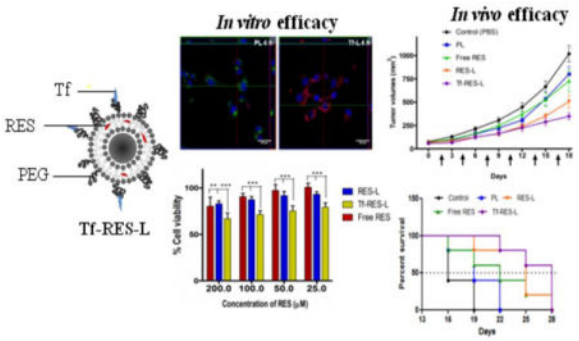

Keywords

Glioblastoma; transferrin; liposomes; resveratrol; targeting; cancer; drug delivery

1. Introduction

Glioblastoma (GBM) is the most lethal of primary malignant brain tumors in adults, and accounts for the majority of all malignant gliomas [1, 2]. In spite of aggressive treatments including surgical resection, radiation and chemotherapy, the median survival for patients post diagnosis is dismal and has remained unchanged at <15 months [2]. Various factors including the molecular and cellular heterogeneity in GBMs, their varying mutation status and the identification of sub-populations of cells known as cancer stem-like cells (CSCs) or tumor- initiating cells (TICs), which drive resistance to conventional chemotherapeutics and radiation resulting in tumor recurrence, further complicate GBM therapy [3–6]. Another substantial hurdle for successful chemotherapy in GBM is the low permeability of the blood-brain barrier (BBB), the tight junction of endothelial cells in the brain, that restricts the systemic delivery of drugs to the brain [7]. This necessitates administration of higher doses of chemotherapeutics to achieve effective concentrations in the brain, which may lead to systemic toxicity, thus severely compromising the quality of life of patients. Moreover, conventional chemotherapeutics often lead to toxicity in normal cells due to their off-target effects. This situation warrants investigation into drugs that are relatively well tolerated and can effectively eliminate GBM.

Resveratrol (3,5,4′-trihydroxystilbene) (RES) is a naturally occurring polyphenol and phytoalexin, found in large quantities in red wine, berries, peanuts and soybeans (Figure 1A). It exhibits pleiotropic health benefits due to its anti-inflammatory, anti-oxidant, anti-carcinogenic, cardio-protective and neuro-protective effects [8–10]. The interest in anti-cancer properties of RES was heightened after its chemopreventive effects were demonstrated at all the stages of cancer including initiation, promotion and progression [11]. RES has been shown to be effective in the treatment of gliomas through a myriad of mechanisms, where it affects both the bulk tumor cells and the glioma stem cells (GSC) or TICs [12–15]. Resveratrol induces apoptosis and suppresses angiogenesis in gliomas by reducing VEGF expression, down-regulates matrix metalloproteinase-9 (MMP-9) expression, enhances radiosensitivity in primary brain TICs, induces autophagy-triggered apoptosis, arrests cell-cycle progression in the S-G2/M phase and induces necrosis in GSCs

at higher doses [12, 13, 15, 16]. Recent studies have also shown that RES improves the apoptosis inducing ability of therapeutics like TRAIL through various mechanisms, and can be used as a sensitizer to other cancer therapeutics [17, 18]. RES potently inhibits both glioma and GSC growth and infiltration by partial deactivation of AKT and p53 induction, resulting in transcription of downstream p53 target genes [19]. In spite of an impressive array of molecular targets and a strong efficacy in gliomas, the therapeutic use of RES is limited due to its poor physico-chemical and pharmacokinetic (PK) properties. It exhibits a high oral absorption (~70%), but a rapid and extensive metabolism resulting in only trace amounts of unchanged drug in the systemic circulation [20]. The poor bioavailability of RES severely compromises its biological and pharmacological benefits. Other limitations of administering RES as a free drug include its poor water solubility, short biological half-life (~9- 14 min for the primary molecule), chemical instability (oxidation and photosensitivity) and a rapid metabolism and elimination [10, 20–22].

A number of drug carriers have been employed to overcome the physico-chemical and pharmacokinetic drawbacks of RES and improve its therapeutic efficacy against various cancers. These include liposomes, micelles, polymeric nanoparticles, solid-lipid nanoparticles and cyclodextrin complexes [8]. Nanocarriers can accumulate passively in tumors by virtue of their size and by taking advantage of the enhanced permeability and retention (EPR) effect [23, 24]. Passive targeting however, suffers from drawbacks that may lead to a non-homogenous distribution of nanocarriers in tumors and may not alone suffice to achieve a therapeutic outcome [25–29]. Active targeting employs nanocarriers decorated with ligands specific for molecules on the tumor cell surface. After extravasation through the tumor vasculature, these nanocarriers can bind to their specific cell targets [30]. Glioblastomas and cancer cells in general proliferate very rapidly compared to normal cells and, as a result, have an increased demand for iron which is required as a cofactor in the synthesis of DNA. Transferrin (Tf), an 80 kDa serum glycoprotein helps in the transfer of iron into growing cells thorough the transferrin receptor (TfR) [31]. Cancer cells show a several-fold higher expression of TfRs to meet this increased demand for iron. The ability of TfR to internalize via clathrin-mediated endocytosis (CME), coupled with its high levels of expression on cancer cells make it a very attractive target for selective drug delivery to malignant cells [32]. Although the BBB restricts the entry for a variety of molecules, large molecules such as insulin and Tf can enter the brain by receptor-mediated endocytosis. The expression of TfR on the BBB makes it attractive for targeted delivery of therapeutic agents to gliomas [32, 33]. The targeting may be achieved by using Tf, the natural ligand to TfR or specific peptides, monoclonal antibodies and single chain antibody fragments to the TfR [34–37].

In the present study, we report on the development of Tf-targeted liposomes loaded with RES for the treatment of glioblastoma. We hypothesized that the Tf-targeted formulations will have greater efficacy than the free drug or the non-targeted liposomes both *in vitro* and *in vivo*. Additionally liposomal encapsulation of RES will protect it in the circulation compared to its administration as a free drug and improve its stability profile.

Recently, Vitamin E -D-α-tocopheryl poly(ethylene glycol) 1000 succinate (TPGS)-coated RES liposomes were studied for their PK and biodistribution in rat brain and were reported

to have superior PK and brain accumulation properties as well as improved *in vitro* cytotoxicity and uptake compared to free RES[38]. Transferrin-modified poly (ethylene glycol)-poly(lactic acid) (PEG-PLA) nanoparticles conjugated to resveratrol have also been reported [39]. The nanoparticles in this study were administered using the intraperitoneal route. A rat glioma cell line was used to evaluate the *in vivo* efficacy of the formulations. The Tf-PEG-PLA-RES nanoparticles were superior to the free drug as shown by the improved *in vitro* and *in vivo* efficacy as well as by the brain accumulation of RES [39]. However, the efficacy of a liposomal system for RES has not yet been studied *in vivo* for GBMs. We explored the possibility of combining the passive targeting ability of long-circulating liposomes and active targeting to TfRs for delivery of RES to GBMs. To our knowledge, this is the first study to report the *in vitro* and *in vivo* efficacy of a Tf-targeted liposomal system for resveratrol in GBMs.

2. Materials

Resveratrol, cholesterol and human holo-transferrin were purchased from Sigma Aldrich (St. Louis, MO). Hoechst 33342, FxCycle™ PI/RNAse staining solution and the ROS indicator 5- (and-6)-chloromethyl-2′,7′-dichlorodihydrofluorescein diacetate acethyl ester (CM-H_2DCFDA) were purchased from Life Technologies/Molecular Probes (Carlsbad, CA). Egg phosphatidylcholine (EggPC), 1,2-dioleoyl-sn-glycero-3-phosphoethanolamine (DOPE), cholesteryl hemisuccinate (CHEMS), and 1,2-dipalmitoyl-*sn*-glycero-3-phosphoethanolamine-N- (lissamine rhodamine B sulfonyl) (Rh-PE) were purchased from Avanti Polar Lipids (Alabaster, AL) and used without further purification.1,2-distearoyl-*sn*-glycero-3-phosphoethanolamine-N- [methoxy(poly(ethylene glycol))-2000] (mPEG-2000-PE) was purchased from Corden Pharma/Genzyme (Cambridge, MA). bis (*p*-nitrophenyl) carbonate polyethylene glycol (NPC- PEG_{3400}-NPC) or (pNP- PEG_{3400}-pNP) was purchased from Laysan Bio (Arab, AL). CellTiter- Blue® cell viability assay reagent and Apo-ONE® Homogeneous Caspase 3/7 assay kit were purchased from Promega (Madison, WI). Anti-transferrin receptor antibody (B-G24)-FITC was purchased from Abcam (Cambridge, MA) and normal mouse IgG1-FITC was purchased from Santa Cruz Biotechnology (Dallas, TX). Micro-BCA protein assay kit, Alexa Fluor® 488 Annexin V/dead cell apoptosis kit and transferrin Alexa Fluor® 680 conjugate were purchased from Thermo Fisher Scientific (Waltham, MA). All other chemicals and solvents were purchased as analytical grade reagents from Thermo Fisher Scientific (Waltham, MA) or Sigma Aldrich (St. Louis, MO) and were used without further purification.

Cell culture

U-87 MG (ATCC® HTB14™), a human glioblastoma, an astrocytoma grade IV cell line was purchased from the American Type Culture Collection (ATCC, Manassas, VA). Dulbecco's modified Eagle's medium (DMEM), Hanks' balanced salt solution (HBSS) (phenol-red free), 0.25% Trypsin-EDTA and penicillin/streptomycin 100X stock solution and CellStripper™ non- enzymatic dissociation solution were purchased from Mediatech, Inc. (Manassas, VA). Primary human astrocytes (HA), astrocyte medium (AM) and poly-L-lysine solution (1 mg/ml) were purchased from ScienCell Research Laboratories (Carlsbad, CA). Heat-inactivated fetal bovine serum (FBS) was purchased from Atlanta Biologicals

(Flowery Branch, GA) and Rocky Mountain Biologicals Inc (Missoula, MT). All adherent cancer cell lines were grown in DMEM supplemented with 10% (v/v) FBS, 50 U/ml penicillin and 50 μg/ml streptomycin (DMEM complete media). The astrocytes were cultured in AM containing 2% FBS and antibiotics. Cells were maintained in a humidified atmosphere of 5% CO_2 at 37°C.

Animals

Female athymic NCr-nu/nu nude mice, (4-6 weeks old), were purchased from Charles River Labs (Wilmington, MA). All animal procedures were performed in accordance with an animal protocol approved by the Northeastern University Institutional Animal Care and Use Committee (NU-IACUC). Mice were housed in groups of 5 at 19-23 °C with a 12 h light-dark cycle and were allowed access to food and water *ad libitum*.

3. Methods

3.1. Preparation of liposomes

Liposomes were prepared using the thin film hydration method [40]. To prepare RES liposomes (RES-L), chloroform solutions of eggPC, cholesterol, DSPE-PEG2000, DOPE and CHEMS (molar ratio 61:24:3:6:6) were added to a round-bottomed flask, along with a solution of RES in methanol. RES was added at a concentration of 3% by weight (3% w/w) to that of the total lipids when forming the film. The organic solvents were evaporated using a Büchi rotavapor R-200 (Büchi, Switzerland) to deposit a thin lipid film on the inner walls of the flask which was freeze dried for at least 4 h using a Labconco freeze dryer (Labconco, Kansas City, MO) to remove traces of the organic solvent. The dried lipid film was hydrated with PBS, pH 7.4 to a final lipid concentration of 10 mg/ml. To prepare unilamellar vesicles, the liposomes were extruded for 21 passages through a mini extruder (Avanti Polar Lipids, Alabaster, AL), using Whatman 200 nm polycarbonate membranes (GE lifesciences, Pittsburgh, PA). The extruded liposomes were filtered through 0.22 μ filters to remove the unincorporated drug and aggregates and to sterilize them for subsequent studies. Plain liposomes (PL) were made without adding RES. In order to fluorescently label the liposomes, 1 mol% Rh-PE was added to the lipids before evaporation of organic solvents, and the drug was excluded (Rh-L). For *in vivo* studies, the lipid concentration was scaled up to 75 mg/ml and the hydration time was increased to improve the incorporation efficiency of RES.

3.2. Preparation of Tf-targeted liposomes

To prepare Tf-targeted liposomes, transferrin moieties were attached to the distal ends of liposome-grafted PEG chains, so that they are free to interact with cells. An amphiphilic PEG derivative pNP-PEG-DOPE was first synthesized as per previously established methods [41]. Briefly, DOPE was mixed with a 5-fold molar excess of NPC-PEG_{3400}-NPC in dry chloroform in the presence of triethylamine. The reaction was stirred overnight at room temperature under nitrogen. Organic solvents were removed by rotary evaporation, followed by freeze-drying to eliminate residual solvents. The dried film was rehydrated with 0.001 N HCl to form micelles. The micelles were separated from unbound PEG and pNP by gel filtration through a Sepharose® CL-4B column using 0.001 N HCl as an eluent. The

fractions were collected and analyzed by thin-layer chromatography on silica gel plates to confirm the pNP-PEG_{3400}-DOPE product. The pure fractions were pooled together and lyophilized. The final lyophilized pNP-PEG_{3400}-DOPE product was weighed, reconstituted in chloroform and stored at −80 °C. To prepare Tf-PEG_{3400}- PE, the pNP-PEG_{3400}-PE (2-fold molar excess over Tf) was taken in a clean glass tube and subjected to evaporation to remove chloroform, followed by freeze-drying to obtain a dry lipid film. The film was rehydrated with 5 mM citrate-buffered saline, pH 5.0, followed by the addition of a solution of transferrin in PBS (pH 8.5). The pH of the solution was adjusted to 8.5-9.0 with 1 N sodium hydroxide, and the reaction was stirred at room temperature overnight. The Tf-PEG_{3400}-PE micelles were then dialyzed against PBS (10 mM, pH 7.4) at room temperature using cellulose ester membranes with a cut-off size of 300 kDa. The amount of Tf in the Tf-PEG_{3400}-PE conjugate was estimated by bicinchoninic acid (BCA) protein assay using bovine serum albumin (BSA) as a standard. Tf was conjugated to the surface of liposomes using the post-insertion method [42]. To prepare Tf-targeted liposomes, RES-L, PL or rhodamine-labeled liposomes (Rh-L) were prepared as mentioned in section 3.1. The prepared liposomes were incubated with requisite amounts of Tf-PEG3400-PE conjugate and placed on a shaker overnight at 37°C to form Tf-targeted PL (Tf-L) or Tf-targeted RES-L (Tf-RES-L).

3.3. Characterization of liposomes

The liposome size (hydrodynamic diameter) was measured by dynamic light scattering (DLS) using a Coulter N4 Plus Submicron Particle Size Analyzer (Coulter Corporation, Miami, FL). Liposome concentration was adjusted to give a light scattering intensity between 5×10^4 and 1×10^6 counts/sec. The zeta-potential was measured using a 90Plus Zeta Phase Analysis Light Scattering (PALS) instrument (Brookhaven Instruments, Holtsville, NY). The liposomes were diluted with deionized distilled water for both the measurements. The amount of RES loaded in the liposomes was determined after filtration of liposomes through a 0.22 μm filter. The wavelength for detection of RES was determined by performing a spectral scan of RES dilutions in methanol in a range of 200-400 nm using a UV mini 1240 UV-Vis spectrophotometer (Shimadzu, Columbia, MD). The RES content was determined at a peak absorption wavelength of 308 ± 2 nm by comparing the concentrations of liposome samples diluted with methanol against a standard curve of RES in methanol. The % drug loaded was determined using the following formula:

$$\%\ \textbf{Drug loaded} = \frac{\text{RES (mg) in the final formulation (final amount)} * 100}{\text{RES (mg) added during liposome preparation (initial amount)}}$$

The size and surface morphology of liposomes was confirmed using TEM analysis. A JEOL JEM-1010 transmission electron microscope (JEOL USA, Inc., Peabody, MA) was used to observe the morphology of liposomes. Briefly, liposome samples (10 μl) were dropped on to a copper grid with formvar and carbon coating, followed by negative staining with 1.5% phosphotungstic acid (PTA). After air-drying at room temperature, the samples were imaged using a transmission electron microscope operating at an accelerating voltage of 80 kV.

3.4. Optimal density of Tf on liposomes for interaction with cells and comparison of Tf-L association between cancer cells and normal cells

To study the influence of ligand density on the interaction of liposomes with cells, Rh-L were prepared and modified with varying densities of Tf (0.05 to 2 mol% of the total lipid concentration). U-87 MG cells (9×10^4 cells/well) seeded in 12 well plates were treated with either Rh-labeled PL or Rh-labeled Tf-modified liposomes at a final lipid concentration of 0.1 mg/ml for 4 h. After 4 h, the formulations were washed off and cells were detached using trypsin-EDTA and collected in 1.5 ml centrifuge tubes. They were centrifuged at 300 × g for 5 min to collect the pellets, which were rinsed twice with ice-cold PBS. Finally, the pellets were re-suspended in 200 μl ice-cold PBS and analyzed by flow cytometry using the BD FACSCalibur™ (Becton Dickinson, Franklin, NJ). The Rh-PE fluorescence was recorded in the FL-2 channel. Cells were gated upon acquisition using forward vs. side scatter to eliminate the dead cells and debris, and 10,000 gated events were collected for each sample. Analysis was performed using the CellQuest ™ Pro software (Becton Dickinson, Franklin, NJ) and the geometric means (GM) of fluorescence were compared among the groups. The density of Tf that showed the maximal association with U-87 MG cells when compared to PL was used for further studies with Tf-L. To compare Tf-L association, between normal and cancer cells, cells (HA and U-87 MG) were cultured in 12-well plates and allowed to adhere until they were 80% confluent. They were treated with either Rh-labeled PL or Tf-L for 4 h. At the end of the treatment, the formulations were removed; cells were washed, trypsinized and processed for flow cytometry to assess the Rh-PE fluorescence as mentioned.

3.5. Involvement of the TfR endocytic pathway in the uptake of Tf-L

To demonstrate that the uptake of Tf-L occurred through the transferrin receptor-mediated endocytic pathway, a competitive inhibition study of Tf-L was carried out in the presence of an excess amount of human holo-transferrin added to the medium. For this study, U-87 MG cells were grown until 80% confluent, and then incubated with 2.5 mg/ml human holo-transferrin solution for 30 min before treating them with Rh-labeled Tf-L. Excess holo-transferrin was incubated with cells throughout the study period of 4 h. The cells were processed for flow cytometry as mentioned in section 3.4 to determine the effect of free transferrin in the media on the interaction of Tf-L with cells. The geometric means of fluorescence in the FL-2 channel were compared between treatments.

3.6. Internalization of Tf-L into GBM cells

Confocal laser scanning microscopy (CLSM) was used to visualize the internalization of Rh-labeled Tf-targeted liposomes by cells. U-87 MG cells (2.5×10^4) were grown on cover-slips placed in 12-well plates until about 70% confluent. The cells were treated with Rh-labeled PL or 1 mol% Tf-L at a final lipid concentration of 0.1mg/ml for 1 h and 4 h respectively. The cells were stained with Hoechst 33342 (5 μg/ml) a nuclear dye, and the endosomal marker Tf-Alexa 680 (5 μg/ml) for 20 min before the liposome treatment was terminated. At the end of the incubation period, cells were rinsed thrice with ice-cold PBS (10 mM), pH 7.4 and fixed with 4% paraformaldehyde for 15 min at room temperature. The cells were rinsed with ice-cold PBS (10 mM), pH 7.4. The cover-slips were mounted on glass slides with

Fluormount-G® medium. The edges of the cover-slips were sealed with a nail lacquer. The slides were observed with a Zeiss LSM 700 inverted confocal microscope (Carl Zeiss Co. Ltd., Jena, Germany) equipped with a 40×, 1.3 numerical aperture plan-apochromat DIC objectives. The z-stack images of the cells (z 1-10, slice thickness 1 μm) were obtained by capturing serial images of the x-y planes by varying the focal length to image along consecutive z-axes. Orthogonal projections were reconstructed from the z-stacks for representation of images using the built-in ZEN software. The LSM images were analyzed using the ImageJ software version 1.43 (NIH, Bethesda, MD). Cellular co- localization was studied with raw images without any further processing.

3.7. Cytotoxicity of RES formulations

To study the cytotoxicity of formulations, U-87 MG cells were seeded at 5×10^3 cells/well and 3×10^3 cells/well for 24 h and 48 h respectively. After an incubation of 24 h at 37 °C and 5% CO_2 the media was replaced with medium containing free RES (in DMSO), RES-L or Tf-RES-L at a RES concentration ranging from 12.5 μM to 200 μM for 4 h in complete DMEM. Liposomes without RES (PL and Tf-L) were used to check the any toxicity from the carrier and untreated cells were used as negative controls. After 4 h, the drug-containing medium was discarded from wells, and cells were washed twice with complete medium. The cells were further incubated for 48 h in 100 μl complete DMEM. A 24 h continuous incubation study was also carried out with the formulations to see if the targeting effect of Tf-RES-L persists for longer incubations in U-87 MG cells. After the designated time points, the cell viability was assessed using the CellTiter- Blue® viability assay as per the manufacturer's instruction. The fluorescence of the plates was read at a wavelength of 530 Ex/590 Em using a Bio-Tek Synergy HT multi-detection micro-plate reader (BioTek, Winooski, VT). The data were analyzed using the Gen5 software (BioTek, Winooski, VT). Statistics were performed on the data obtained from triplicate samples in at least three independent experiments.

3.8. Apoptosis induction

To study the apoptosis induction ability of RES formulations, U-87 MG cells (10^5 cells/well) were seeded in 12-well plates and allowed to attach overnight. They were treated with free RES, RES-L, Tf-RES-L equivalent to a RES concentration of 200 μM, for 24 h to induce apoptosis. Untreated cells were included as controls. The Alexa Fluor® 488 annexin V/dead cell apoptosis kit was used and the manufacturer's protocol was followed for staining the cells. After 24 h, the cells were washed twice with 1X HBSS, pH 7.4 and detached using 0.25% trypsin-EDTA. The cells were collected in 1.5 ml centrifuge tubes and centrifuged at 2000 rpm for 5 min to obtain the cell pellet. The supernatant was discarded and cell pellets were rinsed once with ice-cold PBS, pH 7.4. After discarding the PBS wash, the cell pellets were resuspended in 100 μl, 1X annexin-binding buffer and mixed well. Alexa Fluor®488 (5 μl) and PI working solution (100 μg/ml, 1 μl) were added to each 100 μl cell suspension. The cells were incubated in the dark at room temperature for 15-20 min, after which 400 μl binding buffer was added to all tubes. They were kept on ice and promptly analyzed. The stained cells were analyzed using flow cytometry at an excitation wavelength of 488 nm. The emission of Alexa Fluor®488 was recorded in the FL-1 channel while that of PI was recorded in the FL-3 channel. Cells were gated upon acquisition using

forward vs. side scatter to eliminate the dead cells and debris, and 10,000 gated events were collected for each sample. Analysis was performed using the CellQuest ™ Pro software (Becton Dickinson, Franklin, NJ). The percent of viable, necrotic, late-apoptotic and early-apoptotic cells was determined using quadrant statistics and the percent of gated cells in each quadrant was plotted on a column (bar) graph.

3.9. Caspase 3/7 activity assay

The Apo-ONE® homogeneous caspase 3/7 assay kit was used to study the activation of caspases. U-87 MG cells were seeded at a density of 5×10^3 cells/well and allowed to adhere for 24 h. They were treated for 24 h with RES formulations at concentrations equivalent to 50 and 200 μM in phenol-red free medium. After 24 h, the cells were washed once with serum free media. The caspase substrate was diluted in the Apo-ONE® homogeneous caspase 3/7 buffer, and 50 μl was added to cells containing 50 μl media. The plates were incubated at room temperature in the dark with additional gentle shaking for up to 4 h. After 4 h the fluorescence of each well was read at Ex/Em wavelength of 499/521 using a Bio-Tek Synergy HT multi- detection micro-plate reader (BioTek, Winooski, VT). The data were analyzed using the Gen5 software (BioTek, Winooski, VT). Untreated cells and PL treated cells were used as controls. A blank (media+caspase reagent) reading was subtracted from each reading. The amount of fluorescent product generated was proportional to the amount of caspase 3/7 cleavage activity present in the sample. Data were plotted as the mean fluorescence intensity of each treatment (Mean ± SD).

3.10. Cell cycle analysis

U-87 MG cells (4×10^5) seeded in 6 well plates were treated with free RES (0-300 μM) for 24 h. Untreated cells were used as controls and the DMSO group was the vehicle control. After 24 h, the cells were washed twice with complete DMEM and detached with 0.25 ml trypsin-EDTA. They were collected in 1.5 ml centrifuge tubes and spun at 300 × g for 5 min to obtain a cell pellet. Next, the pellets were washed once, and resuspended in 0.3 ml ice-cold PBS, 10 mM, pH 7.4. The samples were kept on ice during the procedure. The pellets were re-dispersed as single cells by pipetting and fixed with 0.7 ml cold ethanol added drop-wise. The samples were kept on ice for 1 h, and then centrifuged at 0.8 × g for 8 min. Once the cells pelleted, the supernatant was removed, they were washed twice with ice-cold PBS, to ensure complete removal of ethanol. The cell pellets was finally resuspended in 0.3 ml FxCycle™ PI/RNAse staining solution and incubated in the dark at room temperature for 30 min. After 30 min, the DNA content of the samples (PI fluorescence) was analyzed using BD FACSCalibur™ (Becton Dickinson, Franklin, NJ). A total of 10,000 events were collected for each sample. The cells were first gated using the forward vs. side scatter to exclude the dead cells and debris. This gated population was further gated using the FL2-A vs. FL2-W plot to discriminate aggregates or doublets and to include only single cells for cell-cycle analysis. Data was analyzed using the CellQuest™ Pro software (Becton Dickinson, Franklin, NJ). Percentage of gated cells in each phase of the cell cycle was determined from a counts vs. FL2-A histogram and plotted as bar graphs.

3.11. Reactive oxygen species measurement using flow cytometry

U-87 MG or primary human astrocytes were seeded at 10^5cells/well, and allowed to adhere for 24 h. All the treatments were carried out in HBSS (1X), pH 7.4. Following 24 h, the cells were washed once with HBSS and treated with a solution of the ROS-indicator dye CM-H2DCFDA (1 μM) in HBSS for 30 min at 37°C under 5% CO_2, protected from light. After 30 min, the dye- containing medium was removed and the cells were washed twice with HBSS followed by treatment with free RES in DMSO (20- 400 μM) for 1 h. H_2O_2 (500 μM) was used as a positive control in the study. For the comparison with astrocytes, the studies were carried out with free RES (50-400 μM). Cells treated with the dye but not formulations were used to indicate the basal level of ROS in cells. The formulations were incubated with cells for 1 h at 37°C under 5% CO2, protected from light. After 1 h, cells were washed twice with HBSS, and detached using trypsin- EDTA (0.2 ml). Complete DMEM (phenol-red free, 1 ml) was added to the cells to neutralize trypsin and cells were collected in 1.5 ml centrifuge tubes placed on ice. The cells were centrifuged at 300 × g for 5 min to obtain a pellet. The pellet was washed twice and finally resuspended in ice-cold PBS 1X, pH 7.4. Cells were analyzed immediately for ROS levels by flow cytometry using a BD FACSCalibur™ (Becton Dickinson, Franklin, NJ). The green fluorescence of the dye was detected in the FL-1 channel at an emission wavelength of 530 nm. Analysis was performed using the CellQuest ™ Pro software (Becton Dickinson, Franklin, NJ). The graphs were plotted as average fold change in geometric mean over control cells, or alternatively the geometric mean values of fluorescence were compared among groups.

3.12. Tumor growth inhibition study

For this study, U-87 MG cells (2.25×10^6 cells/animal) were injected subcutaneously over the left flank of 4-6 weeks old female athymic NCr-nu/nu nude mice. Once the tumors were between 50-100 mm^3, the animals were randomized into groups (5 animals per group) such that the average tumor volumes were consistent across all the groups. The treatments included PBS pH 7.4, PL (liposomes with no RES), Free RES (6 mg RES dissolved in 20% solution of 2HPβCD), RES-L and Tf-RES-L. The mice were administered injections of formulations containing RES equivalent to 10 mg/kg via the tail vein (injection volumes ≤ 200 μl). The doses were administered every two days once the tumor volumes were between 50-100 mm^3 and tumor measurements were also recorded every third day. The tumor measurements were acquired using a vernier caliper using the formula, tumor volume = [length × (width) ^{2}]/2 where, length is the longer axis of the tumor and width is the measurement perpendicular to the length. The weights of the mice were monitored along with the tumor volumes throughout the study to check for signs of toxicity of administered formulations.

3.13. Survival analysis

The tumor inhibition study was concluded as soon as the average tumor volume of the control animals reached 1000 mm^3. A modified survival analysis was planned for the majority of the animals in other groups that had yet to reach the cut-off volume. The study was thus continued with administration of formulations every third day for a total of up to 10 doses for each group of animals. Tumor volumes were measured every third day as in

section 3.12. The survival end- point for mice was when tumor volume for an animal reached 1000 mm^3, at which point the animal was sacrificed. Kaplan-Meier survival curves were plotted with the percent of animals surviving in each treatment group.

3.14. Statistical analysis

To evaluate statistical significance between groups, one-way ANOVA followed by Tukey's post- hoc test, two-tailed Student's t-tests or Log-rank tests (Mantel-Cox tests) were performed using the GraphPad Prism 5 software (GraphPad Software Inc., San Diego, CA). All numerical data were expressed as mean ±SD or mean ±SEM, with multiple samples from 2-3 independent experiments. The level for statistical significance reported for tests was set at $p < 0.05$. The *, ** and *** in figures indicated p values < 0.05, 0.01 and 0.001 respectively.

4. Results

4.1. Characterization of liposomes

Liposomes were prepared using the thin-film hydration method and RES was loaded passively into liposomes at 3%w/w to the total lipids (10 mg). About 70-75% of the initially added RES was encapsulated within liposomes indicating good drug loading efficiency. Transferrin was attached to the distal end of PEG. The amount of Tf in Tf-PEG_{3400}-PE was quantified by the BCA assay. The reaction efficiency was 60-70%. Different amounts of Tf-PEG_{3400}-PE were added to liposomes using the post-insertion method to optimize the amount of Tf in Tf-L. Table 1 shows the results of characterization of the optimized liposome formulations.

The PL and RES-L were <200 nm with a narrow size distribution. Although addition of Tf increased the liposome sizes by about 20-30 nm, they still maintained a homogeneous distribution. All the liposomes had a negative zeta potential without significant differences between the groups. The formulations for *in vivo* studies were scaled up easily without changes in their particle size and zeta potential values. The increased hydration times led to a 20% increase in drug loading (90%). The TEM studies confirmed the particle size and surface morphology of the liposomes. Negative staining with 1.5% PTA revealed a relatively uniform size distribution of liposomes. The presence of RES did not alter the diameter or surface morphology of liposomes. When compared to PL and RES-L, the surface of Tf-modified liposomes appeared somewhat rougher, probably because of the presence of Tf protein on their surface (Figure 1B). Drug release studies and a long-term stability study were conducted for the unmodified liposomes. The RES-liposomes exhibited excellent stability for a month at 4°C and at room temperature as evidenced from their particle size, zeta potential values and the UV absorbance spectrum of RES (Supp. Table S1 and Supp. Fig. S-1). For the Tf-modified liposomes a short-term stability study was carried out for a period of 8 days over which they remained stable without significant changes in their particle size and zeta potential value (data not shown). Drug release at pH 5.2 and pH 7.4 showed an initially higher release followed by slow sustained release, with higher cumulative release of RES from liposomes at pH 5.2 (Supp. Fig. S-2).

4.2. Transferrin modification significantly improved the association of liposomes with cancer cells

Rhodamine-labeled liposomes prepared with varying densities of Tf-PEG_{3400}-PE were tested for their interaction with U-87 MG cells using flow cytometry. Prior to this study, the over- expression of TfRs on U-87 MG cells was examined by flow cytometry using a FITC labeled anti-TfR antibody (Supp. Fig. S-3). The Tf-Ls at all ligand densities showed a significantly higher association with U-87 MG cells compared to the PL (Figure 2A). Initially with increasing Tf densities, a steady and significant increase in cell association was observed. The maximum cellular association for Tf-L was seen at 1.0 to 1.5 mol% of Tf (GM: 10.6 ± 0.5), which plateaued beyond this point in spite of increasing Tf densities, indicating a possible saturation effect. This reduced association may result from steric hindrance between the ligands or the phenomenon of TfRs existing as “receptor clusters” in cell membranes [43, 44]. There was no statistical difference between the geometric means of fluorescence at 1 to 2 mol% of Tf so the lesser concentration of Tf (1 mol %) was chosen for all further studies. Additional studies showed that although the presence of serum in media decreased association of Tf-L with cells it was still higher than PL, and the association was higher at 4 h than at 1 h (Supp. Fig S 4A and S 4B). For most studies, the 4 h time point was selected and all studies were conducted in serum containing (complete) DMEM.

The association of the optimized TfL formulation was compared between normal cells (primary HA) and cancer cells (U-87 MG). Since both the cell lines are astrocytic in origin, HA represented a good model for comparison. The association of Tf-Ls with cancer cells was significantly higher (~2.3 fold) compared to normal cells as evidenced from their higher geometric mean values of fluorescence in U-87 MG cells (Figure 2B). The association of PL in both cell lines was similar. The Tf-Ls showed a greater targeting and association with U-87 MG cells compared to the normal HA, which was likely due to the higher expression of TfRs on their surface.

4.3. TfR-mediated endocytic pathway was involved in the uptake of Tf-L by cells

Transferrin is taken up by cells via receptor mediated endocytosis (RME) via the transferrin receptors [45]. A competitive inhibition study confirmed that Tf-L undergo the same process of RME to get internalized by cells. Figure 2C shows that in the presence of an excess amount of free holo-transferrin, the association of Tf-L reduces significantly (~2.6 fold decrease), indicating that holo-transferrin is taken up by the process of RME, since adding it prior to treatment with Tf-L blocks the TfRs. As a result, Tf-Ls compete with excess free transferrin in the medium and the association declines due to lack of availability of TfRs. This also proves that the method of internalization of Tf-Ls is indeed through the TfR-mediated endocytosis pathway. The blockage of TfRs did not result in any changes in the interaction of the PL as their association level remained unchanged.

4.4. Transferrin modification enhanced the internalization of liposomes by cancer cells

The intracellular localization of Tf-L was studied using confocal imaging microscopy. To support the conclusion that the liposomes were in fact internalized and not merely associated with the surface of cells, z-stack imaging was carried out. Figure 2D shows representative orthogonal projections reconstructed from the z-stacks showing the XY, YZ and XZ planes

of the image at a specific point. The signal intensity of rhodamine (red channel) was clearly more intense at 4 h compared to 1 h, indicating greater internalization of Tf-L with the longer incubation at 4 h. This also supports the greater association of Tf-L observed at 4 h in the flow cytometry studies (Supp. Fig. S-4C). For PL, the internalization was minimal at both 1 h and 4 h, which suggests that addition of Tf on the liposome surface, does boost association with and internalization of the formulations within cells. At both 1 h and 4 h Tf-Ls internalized to a much greater extent compared to PLs as evidenced by the intense red signal in the cytoplasmic compartment coming from the Rh-labeled liposomes in Figure 2D (Supp. Fig. S-5A and S-5B). For PL at both the time-points, the green signal of Tf-Alexa Fluor® 680 (the endosomal marker) was very bright whereas for the Tf-L treated groups this signal was barely visible, especially at the 4 h time-point (green channel in Fig. S-5A and S-5B). This difference in the endosomal staining between the PL and Tf-L at both the time-points may be attributed to competitive inhibition by the Tf-L. Tf-Alexa fluor 680 internalizes via the TfRs like the Tf-Ls. However, since the dye was incubated for only the last 20 min before the end of incubations, it is very likely that majority of the TfRs were occupied by the Tf-Ls leaving very few receptors for the dye to bind in the Tf-L treated cells. In the case of PLs, the dye could internalize easily, and the endosomes appear bright green since there was no competition from Tf-Ls. This also corroborates the results of the competitive inhibition study in section 4.3.

4.5. Tf-RES-Ls showed a significantly improved cytotoxicity compared to RES-L

At the 24 h time-point, for RES concentrations ≥ 12.5μM, Tf-RES-L were significantly more toxic to cells compared to the RES-L and showed a dose-dependent increase in the cytotoxicity (Figure 3A). At the highest concentration of 200 μM RES, the percent cell viability for RES-L was 61.9 ± 3.9 % where as that for Tf-RES-L was 54.2 ± 3.8 %. Tf-RES-Ls were just as toxic or slightly more toxic to cells compared to the free drug at all but the highest concentration of RES. To better evaluate the targeting effect of Tf-RES-L, a short term cytotoxicity study was also carried out (Figure 3B). The formulations were incubated with cells for 4 h, then washed and further incubated for 48 h before analyzing their cytotoxicity. The superiority of Tf-targeted RES-L was evident during the short-term incubation with cells. At all tested doses of RES, Tf- RES-L showed a significantly higher cytotoxicity compared to either the free RES or untargeted RES-L. At the highest tested concentration, the cell viability was 80.4 ± 9.6 for free RES, 83.0 ± 2.9 for RES-L and 66.9 ± 6.2 for the Tf-RES-L, which was significantly lower than the free RES or RES-L groups. Resveratrol is not considered an extremely potent drug, so with an incubation time of 4 h it is difficult to observe very high toxicities. However, even at 4 h, the Tf-targeted formulation was significantly more toxic than the other groups. The cytotoxicity of RES formulations was also compared between U-87 MG and normal HA (Supp. Fig. S6) and was significantly greater in cancer cells versus the normal cells. This corroborated results from other studies which show selectively greater cytotoxicity of RES to cancer cells compared with normal cells [39, 46].

4.6. RES formulations induced apoptosis in cancer cells accompanied by activation of caspases 3/7

The apoptosis-inducing ability of RES was studied in U-87 MG cells after 24 h treatment with RES formulations. Initiation of apoptosis causes phosphotidyl serine, an early apoptotic marker to translocate from the inner leaflet of the cytoplasmic membrane to the extracellular surface. Fluorescently labeled annexin V binds to this exposed phosphotidyl serine and its fluorescence can be measured by flow cytometry. Propidium iodide (PI) was used in this study to identify the dead cells/necrotic population. Figure 4A shows that Tf-RES-Ls were the most effective in inducing apoptosis in cells at 200 μM. The percentage of early apoptotic cells was 11.6 %, 21.9 % and 34.9 % respectively for free RES, RES-L and Tf-RES-L. Similarly, the percentage of late apoptotic cells was also higher in the Tf-RES-L group (14.4 %) compared to 6.1 % for free RES and 6.5 % for RES-L. Consequently, the percent of viable cells was significantly lower for Tf- RES-L than in other groups. Free RES had 79.7 % and RES-L had 69.6 % viable cells vs. 48 % for the Tf-RES-L group. Thus resveratrol treatment induced apoptosis in U-87 MG cancer cells and the Tf-targeted RES-L induced greater levels of apoptotic cells compared to the free drug or non-targeted RES-L at the same concentrations.

Caspases are key effectors of apoptosis in mammalian cells [47]. Active caspases participate in a cascade of cleavage events that disable key homeostatic and repair enzymes and bring about apoptosis. Caspase activation was studied in U-87 MG cells using the Apo-ONE® homogeneous caspase 3/7 assay. At 200 μM RES, all the treatment groups showed significantly higher caspase 3/7 activity compared to the untreated or PL treated cells (Figure 4B). Significantly higher caspase activation was observed in the Tf-RES-L at the lower concentration (50 μM) compared to free RES and RES-L groups. However, at 200 μM RES, the caspase levels were almost the same in all the three treatment groups. Between 50 and 200 μM, significant differences were seen only for the free RES and RES-L treated cells. For Tf-RES-L the caspase levels were only slightly higher at 200 μM compared to 50 μM. Overall, this study confirmed that the apoptosis observed in U-87 MG cells is accompanied by activation of caspases 3/7.

4.7. Resveratrol led to arrest of cells in the S-phase of the cell cycle, and effectively induced excessive ROS production in cancer cells

Resveratrol induces its effects through a number of different mechanisms in GBM outlined briefly in section 1. RES is frequently reported to bring about an arrest of cells in the S phase, preventing the S-G2/M transition in many different cancer cell lines. The cell-cycle effects of RES were studied in U-87 MG. Untreated cells, and DMSO-treated cells were used as controls. Analysis of the cell-cycle data for U-87 MG revealed that treatment with RES at lower concentrations, in particular, 20 and 50μM significantly arrested the cells in the S-phase of the cell-cycle and stopped their progression to the G2/M phase (Figure 5A). This effect of arrest in S-phase was abrogated at higher concentrations of RES, and the cell-cycle profile at higher concentrations started to resemble the control cells. The representative histograms for DNA content of cells are shown in Supp. Fig. S7. An increase in the percentage of cells in the S-phase at 20 and 50 μM also brought about a corresponding significant decrease in cells in the G0/G1 phase compared to other groups. The cell-cycle

profile at all the other tested concentrations showed a low percentage of S-phase cells and a higher percentage of G2/M phase cells. These results demonstrate that RES inhibits the S to G2/M progression of cells, albeit at lower concentrations only.

ROS generation has been described as one of the mechanisms for RES toxicity in cancer cells [48]. This study was undertaken to determine if RES affected ROS production in GBM cell lines. Hydrogen peroxide, the endogenous ROS, was used as a positive control in this study. DMSO was the vehicle control, and cells treated with only the dye CM-H_2DCFDA were used as the negative control. Upon oxidation by ROS, the non fluorescent CM-H_2DCFDA is converted to the highly fluorescent DCF which can be detected by any fluorescence method. As seen in Figure 5B, RES treatments induced ROS production in U-87 MG cells after just 1 h of treatment. A dose-dependent increase was observed in the cellular ROS levels. At the higher concentrations of 200 and 400 μM RES, the increases in ROS levels (~6-fold and 16-fold respectively) were significantly higher than basal ROS levels in the cells (dye-treated control group: Ctrl+dye). The ROS levels for the positive control treatment (H_2O_2) were significantly (~7-fold) higher than the basal levels. The ROS levels were also compared between cancer cells (U-87 MG) and normal cells (HA) (Supp. Fig. S8). At higher doses, significantly higher levels of ROS were generated in cancer cells compared to the normal HA, indicating the selectivity of RES, and its enhanced ability to act as a pro-oxidant in cancer cells. The effects of RES on the normal astrocytes were relatively milder compared to those on cancer cells, indicating the vulnerability of cancer cells to RES-induced increase in the oxidative stress burden.

4.8. Liposomal formulations of RES improved tumor growth inhibition and survival in U-87 MG tumor xenograft-bearing mice

The tumor-inhibition study was conducted over a period of 18 days and was concluded when the average tumor volume of control animals reached 1000 mm^3. Six doses of the formulations were administered over this period. From Figure 6A (Supp. Fig. S9), it was clear that Tf-RES-L were more effective in controlling the tumor growth compared to the other groups. The volumes of Tf- RES-L treated tumors were significantly less than the PBS, PL or free RES treated tumors respectively. The RES-L treated tumors also had a significantly lower volume compared to the PBS or PL treated tumors. The average tumor volumes (± SEM) at the end of the study were 1018.8 ± 87.5 $mm^3$for PBS treated control tumors, 802.0 ± 83.4 $mm^3$for PL, 728.2 ± 117.9 $mm^3$for free RES, 506.9 ± 69.6 $mm^3$for RES-L and 349.3 ± 38.1 mm^3 for the Tf-RES-L treated tumors. Although the tumor volumes were much lower for RES-L compared to free RES, the difference was not statistically significant at the end of the study (day 18). However, statistically lower tumor volumes were observed on days 9 and 12 of the study. The Tf-RES-L treated tumors were significantly smaller than free RES treated tumors from day 12 until the end of the study. Throughout the study, the tumor volumes for the RES-L group were slightly higher than the Tf- RES-L treated group. The encapsulation of resveratrol within liposomes definitely helped compared to administration of free RES. However, large differences were not seen between the free drug and RES-L. Adding Tf to the liposomes improved the efficacy of RES-L and inhibited tumor growth significantly compared to the PBS, PL or free RES-treated tumors. There were no significant weight changes in animals among all the treatment groups during study

period, indicating minimum or total lack of apparent toxicity of the administered formulations (Figure 6B).

A modified survival analysis was performed by defining the survival end-point as the time taken for the tumor volume of a mouse to reach 1000 mm^3. Additional doses were administered to the animals included in the tumor-inhibition study every third day for a total of 10 doses or until their tumor volumes reached the cut-off mark. The tumors from RES-L and Tf-RES-L treated groups took longer to reach the survival end-point volume of 1000 mm^3, and these mice survived significantly longer compared to the PBS and PL treated groups (Figure 6C).

No significant differences were observed between free RES and the PBS or PL treated groups. The Tf-RES-L were somewhat superior compared to the other treatments in terms of the percent animals surviving (Figure 6D). At day 25, only 20% of the animals in free RES and RES-L treatment groups were still to reach the tumor volume cut-off of 1000 mm^3. But in the Tf-RES-L group 60% of the animals were yet to reach that stage. All the PBS-treated and PL-treated mice were sacrificed at day 16 and day 19 respectively. The median survival for all the groups was: Control (PBS) 16 days, PL 19 days, free RES 22 days, RES-L 25 days and Tf-RES-L 28 days (Figure 6D). The *in vivo* studies show that RES-L and Tf-RES-L were more effective in controlling the growth of U-87 MG tumors in nude mice compared to other groups. Moreover addition of Tf to RES-L further improved their efficacy significantly over administering the free drug.

5.0. Discussion

The treatment of GBMs remains an unmet medical need in spite of the current aggressive therapeutic regimens. Resveratrol, a natural polyphenol has been shown to be effective in GBMs and other cancers by acting through a myriad of mechanisms. In spite of its pleiotropic health benefits and an excellent safety profile, the poor physicochemical characteristics of RES severely limit its use as a free drug. The goal of this work was to develop a liposomal formulation of RES to overcome its limitations as a free drug, and to enhance its solubility and stability. We hypothesized that modifying liposomes with transferrin, the natural ligand of TfRs over- expressed in many cancers including GBMs will further improve the efficacy of RES-L both *in vitro* and *in vivo*. So far, studies with RES formulations and more specifically studies investigating the *in vitro* and *in vivo* efficacy of RES-loaded liposomes in GBMs have not yet been explored.

Resveratrol was successfully encapsulated within liposomes, and exhibited a good encapsulation efficiency of about 75%. The RES-L exhibited a homogeneous size distribution with a negative zeta potential (Table 1), were stable for a month at room temperature and at 4°C, and could be scaled-up easily for *in vivo* studies. The Tf-L showed significantly higher association with cancer cells compared to normal human astrocytes, most likely due to upregulation of TfRs in cancer cells (Figure 2B). The increased association translated into greater cellular internalization of Tf-L compared to PL which was confirmed using confocal microscopy (Figure 2D). Competitive inhibition in the presence of excess of free transferrin confirmed that Tf-Ls utilized the TfR-mediated endocytosis

pathway to internalize into cells (Figure 2C). The inclusion of CHEMS and DOPE in the liposomes possibly assisted in the endosomal escape of liposomes that enter through the TfR-mediated endocytic pathway, by delivering more cargo inside cells. The enhanced cellular association and internalization of Tf-L also translated into improved cytotoxicity of Tf-RES-L. The benefits of Tf-targeting were evident during short-term incubation studies (4 h) where Tf-RES-L exhibited a significantly higher cytotoxicity at all the tested concentrations compared to both free RES and RES-L (Figure 3B). However, continuous incubation for 24 h did not show the benefit of targeting at the highest tested concentration (Figure 3A). In static culture conditions, the continuous availability of high concentrations of free RES to cells at a time may overshadow the slow release of drug from liposomes, outweighing the benefits of targeting over 24 h. However, significantly higher toxicity was seen for Tf-RES-L at low concentrations (<100 μM) even during the continuous incubation. In general, the overall cytotoxicity with RES is not as high as with the conventional chemotherapeutics, but these studies do support to a certain extent the importance of improving the efficacy of RES by addition of a targeting ligand such as Tf to RES-L.

One of the mechanisms of RES-induced cytotoxicity was its apoptosis-inducing ability in the cancer cells, which was accompanied by activation of caspase 3/7, the key effectors in the apoptotic process (Figure 4). The Tf-RES-L showed a significantly greater apoptosis-inducing ability compared to free RES and RES-L. A higher caspase 3/7 activity was observed for Tf- RES-L compared to the other groups at the low RES concentration (50 μM) but at 200 μM the caspase activity was similar between the groups. Further evaluations at shorter time-points may be needed to accurately comment on the differences observed in these assays at different RES concentrations. Cell-cycle studies in U-87 MG showed that, low RES concentrations (<75 μM), can cause a significant arrest of cells in the S phase of the cell-cycle preventing their S to G2/M transition (Figure 5A). Resveratrol forced the cells from a quiescent state in G0/G1 phase into the S-phase and eventually resulted in their death. This prompted further investigation into other mechanisms of RES, including its ability to induce oxidative stress in cells (Figure 5B). Significant levels of reactive oxygen species (ROS) were generated in U-87 MG cells at RES concentrations ≥ 100 μM after just 1 h treatment with free RES, suggesting that the cytotoxic actions of RES could be a result of its pro-oxidant effect on cancer cells as was also observed in other studies [48–50]. Some studies have also shown that in the presence of ROS scavengers like N-acetyl-L- cysteine, the ROS production by RES is decreased significantly which ultimately decreases the ability of RES to induce apoptosis [50, 51]. The basal ROS levels in cancer cells are much higher than the normal cells, and they play a role in cancer progression [52, 53]. Cancer cells, unlike normal cells operate very close to the threshold capacity of their anti-oxidant systems to eliminate ROS, which allows exogenous pro-oxidants (like RES) to selectively induce excessive ROS in cancer cells by overwhelming their anti-oxidant systems [54]. Also, RES generated significantly higher levels of ROS selectively in U-87 MG but not HA (Supp. Fig S8). This preferential effect of RES on ROS levels showed that at concentrations that could damage cancer cells, RES was quite safe to administer to normal cells. Overall, the *in vitro* results show that, to a great extent, the effectiveness of RES-L benefitted from surface modification with transferrin.

The final goal was to test the efficacy of RES formulations *in vivo*. To encapsulate RES and administer it at a dose of 10 mg/kg, the liposome formulation was scaled up substantially from the *in vitro* studies (10 mg/ml to 75 mg/ml). A higher drug-loading efficiency was achieved by increasing the hydration time, with no change in other physico-chemical parameters of liposomes, which confirmed the scalability of the liposomal formulations, a critical aspect for translation. The tumor-inhibition studies showed a trend where, Tf-RES-L treated mice had the smallest tumors compared to all the other comparison groups. Both the liposomal formulations were significantly better than the PBS-treated animals throughout the study (Figure 6A); whereas there were no differences in the tumor volumes for free RES and PBS treated mice on any day. This was expected, given the short half-life of free RES although it was administered as a complex in 2HPβCD. While 2HPβCD acted as a vehicle, it may not afford adequate protection to RES in the circulation, allowing it to be metabolized quickly, with loss of its activity. In the drug release studies, free RES was released from the complex in 1.5-2 h compared to over 72 h from long-circulating liposomes, which may lead to more liposomal RES at the tumor site. However, biodistribution studies need to be done to conclusively show whether RES-L indeed accumulate to a greater extent in the tumors. Interestingly, significant differences could not be established between RES-L and Tf-RES-L during the study, although the difference in tumor volumes increased towards the study's end. One possible explanation is that *in vivo*, passive targeting and the EPR effect may enable enough RES-L to enter the tumor, and overshadow the benefits of adding a ligand like Tf. An alternative explanation can be based on the results reported from a study with silicon dioxide (SiO_2) nanoparticles (NPs) grafted with Tf on the surface [55]. It reported that the specific targeting ability of Tf-targeted NPs is lost when placed in a complex biological environment due to the formation of a protein corona that screens the targeting molecules on the surface [55]. We did observe a decline in the association of Tf-L with cells in the presence of 10% FBS (Supp. Fig. 4B), but additional studies are needed to extrapolate the results conclusively to *in vivo* conditions. In this case, the Tf-targeting ability was not totally lost, since our *in vivo* results definitely show that Tf-RES-L treated mice had smaller tumors compared to other groups at the end of the study. However, none of the treatments could completely abolish tumor growth. The potency of RES is lower than traditional chemotherapeutics, and it is likely that RES was not able to effectively control tumor growth at the dose that it was administered in this study. The *in vivo* effects may be enhanced by more frequent dosing (everyday instead of every third day), early initiation of the treatment (at the time of tumor inoculation or immediately after it instead of allowing tumors to grow to 50-100 mm^3) and increasing the dose of the drug. Compared to RES conjugated PEG-PLA nanocarriers and vitamin E-TPGS-coated liposomes investigated for RES delivery in GBMs, the liposomes used in this study are larger in size [19, 56]. The *in vivo* evaluations in this study employed a subcutaneous xenograft versus an orthotopic model employed in the study by Guo et al. [39]. For future investigations in orthotopic models, the size of liposomes needs to be closer to 100 nm. Although, this study did show the benefit of encapsulating RES in liposomes targeted with Tf and administering it i.v for GBM treatment at a dose of 10 mg/kg compared to 15 mg/kg employed for the Tf-PEG-PLA nanoparticles conjugated with RES.

Importantly, in a modified survival study where a tumor-volume of 1000 mm^3 was the end-point, Tf-RES-L treated mice showed an improved median survival (Figure 6C and 6D). In this study, the percentage of animals surviving at day 25 (yet to reach the 1000 mm^3) was the highest for Tf-RES-L (60%) compared to only 20% for RES-L and free RES. These *in vivo* studies have laid the basic groundwork to show the initial proof of concept for efficacy of liposomal formulations of RES.

6.0. Conclusion

The search for non-conventional chemotherapeutic agents has been spurred by the shortcomings of conventional chemotherapeutics such as the development of resistance and unwanted side-effects in normal tissues. Resveratrol has shown efficacy in the treatment of cancers, but suffers from physico-chemical limitations that restrict its use as a free drug. In the past two years, a number of studies have evaluated RES-loaded in liposomes either as a single agent or in combination with other drugs like paclitaxel, doxorubicin, 5-FU or curcumin for various cancers [56–60]. To our knowledge, this is the first study to investigate liposomes loaded with RES and targeted using the natural ligand, transferrin, to GBM cells. The RES-liposomes developed in this project were robust, versatile and scalable. However, additional studies addressing their biodistribution and PK properties *in vivo* and their ability to cross the BBB need to be carried out to fully characterize them. Combinations of RES with other natural agents like curcumin, quercetin, genistein or other drugs encapsulated within liposomes may further improve the treatment efficacy. Resveratrol is effective against many cancers and Tf is overexpressed on a majority of cancer cells. Thus, Tf-targeted RES-loaded liposomes may prove to be an effective nanomedicine in a wide range of cancers. The preliminary results thus far are encouraging in that they extend the utility of these liposomal formulations to other cancers as well.

To conclude, the Tf-RES-L developed in this project showed an enhanced *in vitro* activity, which translated into to a favorable therapeutic response *in vivo* compared to the free drug and non-targeted RES-L. Finally, one of the critical aspects of this work was the use of a non- conventional and relatively safe drug to treat GBMs. To a great extent, these results justify the optimism about resveratrol as an important addition in the treatment of GBMs.

Supplementary Material

Refer to Web version on PubMed Central for supplementary material.

Acknowledgments

The authors thank William Fowle for his help with TEM imaging and William C. Hartner for his help in editing the manuscript.

Funding sources

This study was funded from the overhead return account of VT.

References

1. Ostrom QT, Gittleman H, Liao P, Rouse C, Chen Y, Dowling J, Wolinsky Y, Kruchko C, Barnholtz-Sloan J. CBTRUS statistical report: primary brain and central nervous system tumors diagnosed in the United States in 2007-2011. Neuro Oncol. 2014; 16(Suppl 4):iv1–63. [PubMed: 25304271]
2. Stupp R, Hegi ME, Mason WP, van den Bent MJ, Taphoorn MJ, Janzer RC, Ludwin SK, Allgeier A, Fisher B, Belanger K, Hau P, Brandes AA, Gijtenbeek J, Marosi C, Vecht CJ, Mokhtari K, Wesseling P, Villa S, Eisenhauer E, Gorlia T, Weller M, Lacombe D, Cairncross JG, Mirimanoff RO. Effects of radiotherapy with concomitant and adjuvant temozolomide versus radiotherapy alone on survival in glioblastoma in a randomised phase III study: 5-year analysis of the EORTC-NCIC trial. Lancet Oncol. 2009; 10:459–466. [PubMed: 19269895]
3. Friedmann-Morvinski D. Glioblastoma heterogeneity and cancer cell plasticity. Crit Rev Oncog. 2014; 19:327–336. [PubMed: 25404148]
4. Liu A, Hou C, Chen H, Zong X, Zong P. Genetics and Epigenetics of Glioblastoma: Applications and Overall Incidence of IDH1 Mutation. Front Oncol. 2016; 6:16. [PubMed: 26858939]
5. Singh SK, Hawkins C, Clarke ID, Squire JA, Bayani J, Hide T, Henkelman RM, Cusimano MD, Dirks PB. Identification of human brain tumour initiating cells. Nature. 2004; 432:396–401. [PubMed: 15549107]
6. Bao S, Wu Q, McLendon RE, Hao Y, Shi Q, Hjelmeland AB, Dewhirst MW, Bigner DD, Rich JN. Glioma stem cells promote radioresistance by preferential activation of the DNA damage response. Nature. 2006; 444:756–760. [PubMed: 17051156]
7. Banks WA. From blood-brain barrier to blood-brain interface: new opportunities for CNS drug delivery. Nat Rev Drug Discov. 2016; 15:275–292. [PubMed: 26794270]
8. Neves AR, Lucio M, Lima JL, Reis S. Resveratrol in medicinal chemistry: a critical review of its pharmacokinetics, drug-delivery, and membrane interactions. Curr Med Chem. 2012; 19:1663–1681. [PubMed: 22257059]
9. Catalgol B, Batirel S, Taga Y, Ozer NK. Resveratrol: French paradox revisited. Front Pharmacol. 2012; 3:141. [PubMed: 22822401]
10. Baur JA, Sinclair DA. Therapeutic potential of resveratrol: the in vivo evidence. Nat Rev Drug Discov. 2006; 5:493–506. [PubMed: 16732220]
11. Jang M, Cai L, Udeani GO, Slowing KV, Thomas CF, Beecher CW, Fong HH, Farnsworth NR, Kinghorn AD, Mehta RG, Moon RC, Pezzuto JM. Cancer chemopreventive activity of resveratrol, a natural product derived from grapes. Science. 1997; 275:218–220. [PubMed: 8985016]
12. Castino R, Pucer A, Veneroni R, Morani F, Peracchio C, Lah TT, Isidoro C. Resveratrol reduces the invasive growth and promotes the acquisition of a long-lasting differentiated phenotype in human glioblastoma cells. J Agric Food Chem. 2011; 59:4264–4272. [PubMed: 21395220]
13. Filippi-Chiela EC, Villodre ES, Zamin LL, Lenz G. Autophagy interplay with apoptosis and cell cycle regulation in the growth inhibiting effect of resveratrol in glioma cells. PLoS One. 2011; 6:e20849. [PubMed: 21695150]
14. Sato A, Okada M, Shibuya K, Watanabe E, Seino S, Suzuki K, Narita Y, Shibui S, Kayama T, Kitanaka C. Resveratrol promotes proteasome-dependent degradation of Nanog via p53 activation and induces differentiation of glioma stem cells. Stem Cell Res. 2013; 11:601–610. [PubMed: 23651583]
15. Yang YP, Chang YL, Huang PI, Chiou GY, Tseng LM, Chiou SH, Chen MH, Chen MT, Shih YH, Chang CH, Hsu CC, Ma HI, Wang CT, Tsai LL, Yu CC, Chang CJ. Resveratrol suppresses tumorigenicity and enhances radiosensitivity in primary glioblastoma tumor initiating cells by inhibiting the STAT3 axis. Journal of Cellular Physiology. 2012; 227:976–993. [PubMed: 21503893]
16. Tseng SH, Lin SM, Chen JC, Su YH, Huang HY, Chen CK, Lin PY, Chen Y. Resveratrol suppresses the angiogenesis and tumor growth of gliomas in rats. Clin Cancer Res. 2004; 10:2190–2202. [PubMed: 15041740]
17. Mitchell MJ, Webster J, Chung A, Guimaraes PP, Khan OF, Langer R. Polymeric mechanical amplifiers of immune cytokine-mediated apoptosis. Nat Commun. 2017; 8:14179. [PubMed: 28317839]

18. Ganapathy S, Chen Q, Singh KP, Shankar S, Srivastava RK. Resveratrol enhances antitumor activity of TRAIL in prostate cancer xenografts through activation of FOXO transcription factor. PLoS One. 2010; 5:e15627. [PubMed: 21209944]
19. Clark PA, Bhattacharya S, Elmayan A, Darjatmoko SR, Thuro BA, Yan MB, van Ginkel PR, Polans AS, Kuo JS. Resveratrol targeting of AKT and p53 in glioblastoma and glioblastoma stem-like cells to suppress growth and infiltration. J Neurosurg. 2016:1–13.
20. Walle T, Hsieh F, DeLegge MH, Oatis JE, Walle UK. High absorption but very low bioavailability of oral resveratrol in humans. Drug Metabolism and Disposition. 2004; 32:1377–1382. [PubMed: 15333514]
21. Asensi M, Medina I, Ortega A, Carretero J, Bano MC, Obrador E, Estrela JM. Inhibition of cancer growth by resveratrol is related to its low bioavailability. Free Radic Biol Med. 2002; 33:387–398. [PubMed: 12126761]
22. Marier JF, Vachon P, Gritsas A, Zhang J, Moreau JP, Ducharme MP. Metabolism and disposition of resveratrol in rats: extent of absorption, glucuronidation, and enterohepatic recirculation evidenced by a linked-rat model. J Pharmacol Exp Ther. 2002; 302:369–373. [PubMed: 12065739]
23. Maeda H, Wu J, Sawa T, Matsumura Y, Hori K. Tumor vascular permeability and the EPR effect in macromolecular therapeutics: a review. J Control Release. 2000; 65:271–284. [PubMed: 10699287]
24. Matsumura Y, Maeda H. A new concept for macromolecular therapeutics in cancer chemotherapy: mechanism of tumoritropic accumulation of proteins and the antitumor agent smancs. Cancer Res. 1986; 46:6387–6392. [PubMed: 2946403]
25. Fang J, Nakamura H, Maeda H. The EPR effect: Unique features of tumor blood vessels for drug delivery, factors involved, and limitations and augmentation of the effect. Adv Drug Deliv Rev. 2011; 63:136–151. [PubMed: 20441782]
26. Hatakeyama H, Akita H, Harashima H. A multifunctional envelope type nano device (MEND) for gene delivery to tumours based on the EPR effect: a strategy for overcoming the PEG dilemma. Adv Drug Deliv Rev. 2011; 63:152–160. [PubMed: 20840859]
27. Heldin CH, Rubin K, Pietras K, Ostman A. High interstitial fluid pressure - an obstacle in cancer therapy. Nat Rev Cancer. 2004; 4:806–813. [PubMed: 15510161]
28. Hobbs SK, Monsky WL, Yuan F, Roberts WG, Griffith L, Torchilin VP, Jain RK. Regulation of transport pathways in tumor vessels: role of tumor type and microenvironment. Proc Natl Acad Sci U S A. 1998; 95:4607–4612. [PubMed: 9539785]
29. Prabhakar U, Maeda H, Jain RK, Sevick-Muraca EM, Zamboni W, Farokhzad OC, Barry ST, Gabizon A, Grodzinski P, Blakey DC. Challenges and Key Considerations of the Enhanced Permeability and Retention Effect for Nanomedicine Drug Delivery in Oncology. Cancer Res. 2013; 73:2412–2417. [PubMed: 23423979]
30. Jhaveri A, Torchilin V. Intracellular delivery of nanocarriers and targeting to subcellular organelles. Expert Opin Drug Deliv. 2016; 13:49–70. [PubMed: 26358656]
31. Singh M. Transferrin As A targeting ligand for liposomes and anticancer drugs. Curr Pharm Des. 1999; 5:443–451. [PubMed: 10390608]
32. Daniels TR, Delgado T, Rodriguez JA, Helguera G, Penichet ML. The transferrin receptor part I: Biology and targeting with cytotoxic antibodies for the treatment of cancer. Clin Immunol. 2006; 121:144–158. [PubMed: 16904380]
33. Calzolari A, Larocca LM, Deaglio S, Finisguerra V, Boe A, Raggi C, Ricci-Vitani L, Pierconti F, Malavasi F, De Maria R, Testa U, Pallini R. Transferrin receptor 2 is frequently and highly expressed in glioblastomas. Transl Oncol. 2010; 3:123–134. [PubMed: 20360937]
34. Crepin R, Goenaga AL, Jullienne B, Bougherara H, Legay C, Benihoud K, Marks JD, Poul MA. Development of human single-chain antibodies to the transferrin receptor that effectively antagonize the growth of leukemias and lymphomas. Cancer Res. 2010; 70:5497–5506. [PubMed: 20530676]
35. Kawamoto M, Horibe T, Kohno M, Kawakami K. A novel transferrin receptor-targeted hybrid peptide disintegrates cancer cell membrane to induce rapid killing of cancer cells. BMC Cancer. 2011; 11:359. [PubMed: 21849092]

36. Loureiro JA, Gomes B, Fricker G, Cardoso I, Ribeiro CA, Gaiteiro C, Coelho MA, Pereira MD, Rocha S. Dual ligand immunoliposomes for drug delivery to the brain. Colloids Surf B Biointerfaces. 2015; 134:213–219. [PubMed: 26204501]
37. Sawant RR, Jhaveri AM, Koshkaryev A, Zhu L, Qureshi F, Torchilin VP. Targeted transferrin-modified polymeric micelles: enhanced efficacy in vitro and in vivo in ovarian carcinoma. Mol Pharm. 2014; 11:375–381. [PubMed: 24325630]
38. Vijayakumar MR, Vajanthri KY, Balavigneswaran CK, Mahto SK, Mishra N, Muthu MS, Singh S. Pharmacokinetics, biodistribution, in vitro cytotoxicity and biocompatibility of Vitamin E TPGS coated trans resveratrol liposomes. Colloids Surf B Biointerfaces. 2016; 145:479–491. [PubMed: 27236510]
39. Guo W, Li A, Jia Z, Yuan Y, Dai H, Li H. Transferrin modified PEG-PLA-resveratrol conjugates: in vitro and in vivo studies for glioma. Eur J Pharmacol. 2013; 718:41–47. [PubMed: 24070814]
40. Bangham AD, Standish MM, Watkins JC. Diffusion of univalent ions across the lamellae of swollen phospholipids. J Mol Biol. 1965; 13:238–252. [PubMed: 5859039]
41. Torchilin VP, Levchenko TS, Lukyanov AN, Khaw BA, Klibanov AL, Rammohan R, Samokhin GP, Whiteman KR. p-Nitrophenylcarbonyl-PEG-PE-liposomes: fast and simple attachment of specific ligands, including monoclonal antibodies, to distal ends of PEG chains via p-nitrophenylcarbonyl groups. Biochim Biophys Acta. 2001; 1511:397–411. [PubMed: 11286983]
42. Allen TM, Sapra P, Moase E. Use of the post-insertion method for the formation of ligand-coupled liposomes. Cell Mol Biol Lett. 2002; 7:217–219. [PubMed: 12097921]
43. Gullotti E, Yeo Y. Extracellularly activated nanocarriers: a new paradigm of tumor targeted drug delivery. Mol Pharm. 2009; 6:1041–1051. [PubMed: 19366234]
44. Liu AP, Aguet F, Danuser G, Schmid SL. Local clustering of transferrin receptors promotes clathrin-coated pit initiation. J Cell Biol. 2010; 191:1381–1393. [PubMed: 21187331]
45. Cheng Y, Zak O, Aisen P, Harrison SC, Walz T. Structure of the human transferrin receptor-transferrin complex. Cell. 2004; 116:565–576. [PubMed: 14980223]
46. Vinod BS, Nair HH, Vijayakurup V, Shabna A, Shah S, Krishna A, Pillai KS, Thankachan S, Anto RJ. Resveratrol chemosensitizes HER-2-overexpressing breast cancer cells to docetaxel chemoresistance by inhibiting docetaxel-mediated activation of HER-2-Akt axis. Cell Death Discov. 2015; 1:15061. [PubMed: 27551486]
47. Nicholson DW, Ali A, Thornberry NA, Vaillancourt JP, Ding CK, Gallant M, Gareau Y, Griffin PR, Labelle M, Lazebnik YA, et al. Identification and inhibition of the ICE/CED-3 protease necessary for mammalian apoptosis. Nature. 1995; 376:37–43. [PubMed: 7596430]
48. Seino M, Okada M, Shibuya K, Seino S, Suzuki S, Takeda H, Ohta T, Kurachi H, Kitanaka C. Differential contribution of ROS to resveratrol-induced cell death and loss of self- renewal capacity of ovarian cancer stem cells. Anticancer Res. 2015; 35:85–96. [PubMed: 25550538]
49. Luo H, Yang A, Schulte BA, Wargovich MJ, Wang GY. Resveratrol induces premature senescence in lung cancer cells via ROS-mediated DNA damage. PLoS One. 2013; 8:e60065. [PubMed: 23533664]
50. Miki H, Uehara N, Kimura A, Sasaki T, Yuri T, Yoshizawa K, Tsubura A. Resveratrol induces apoptosis via ROS-triggered autophagy in human colon cancer cells. Int J Oncol. 2012; 40:1020–1028. [PubMed: 22218562]
51. Gu S, Chen C, Jiang X, Zhang Z. ROS-mediated endoplasmic reticulum stress and mitochondrial dysfunction underlie apoptosis induced by resveratrol and arsenic trioxide in A549 cells. Chem Biol Interact. 2016; 245:100–109. [PubMed: 26772155]
52. Toyokuni S, Okamoto K, Yodoi J, Hiai H. Persistent oxidative stress in cancer. FEBS Lett. 1995; 358:1–3. [PubMed: 7821417]
53. Wu WS. The signaling mechanism of ROS in tumor progression. Cancer Metastasis Rev. 2006; 25:695–705. [PubMed: 17160708]
54. Pelicano H, Carney D, Huang P. ROS stress in cancer cells and therapeutic implications. Drug Resist Updat. 2004; 7:97–110. [PubMed: 15158766]
55. Salvati A, Pitek AS, Monopoli MP, Prapainop K, Bombelli FB, Hristov DR, Kelly PM, Aberg C, Mahon E, Dawson KA. Transferrin-functionalized nanoparticles lose their targeting capabilities

when a biomolecule corona adsorbs on the surface. Nat Nanotechnol. 2013; 8:137–143. [PubMed: 23334168]

56. Kim SH, Adhikari BB, Cruz S, Schramm MP, Vinson JA, Narayanaswami V. Targeted intracellular delivery of resveratrol to glioblastoma cells using apolipoprotein E- containing reconstituted HDL as a nanovehicle. PLoS One. 2015; 10:e0135130. [PubMed: 26258481]
57. Catania A, Barrajon-Catalan E, Nicolosi S, Cicirata F, Micol V. Immunoliposome encapsulation increases cytotoxic activity and selectivity of curcumin and resveratrol against HER2 overexpressing human breast cancer cells. Breast Cancer Res Treat. 2013; 141:55–65. [PubMed: 23959397]
58. Meng J, Guo F, Xu H, Liang W, Wang C, Yang XD. Combination Therapy using Co- encapsulated Resveratrol and Paclitaxel in Liposomes for Drug Resistance Reversal in Breast Cancer Cells in vivo. Sci Rep. 2016; 6:22390. [PubMed: 26947928]
59. Mohan A, Narayanan S, Balasubramanian G, Sethuraman S, Krishnan UM. Dual drug loaded nanoliposomal chemotherapy: A promising strategy for treatment of head and neck squamous cell carcinoma. Eur J Pharm Biopharm. 2016; 99:73–83. [PubMed: 26690333]
60. Mohan A, Narayanan S, Sethuraman S, Krishnan UM. Novel resveratrol and 5- fluorouracil coencapsulated in PEGylated nanoliposomes improve chemotherapeutic efficacy of combination against head and neck squamous cell carcinoma. Biomed Res Int. 2014; 2014:424239. [PubMed: 25114900]

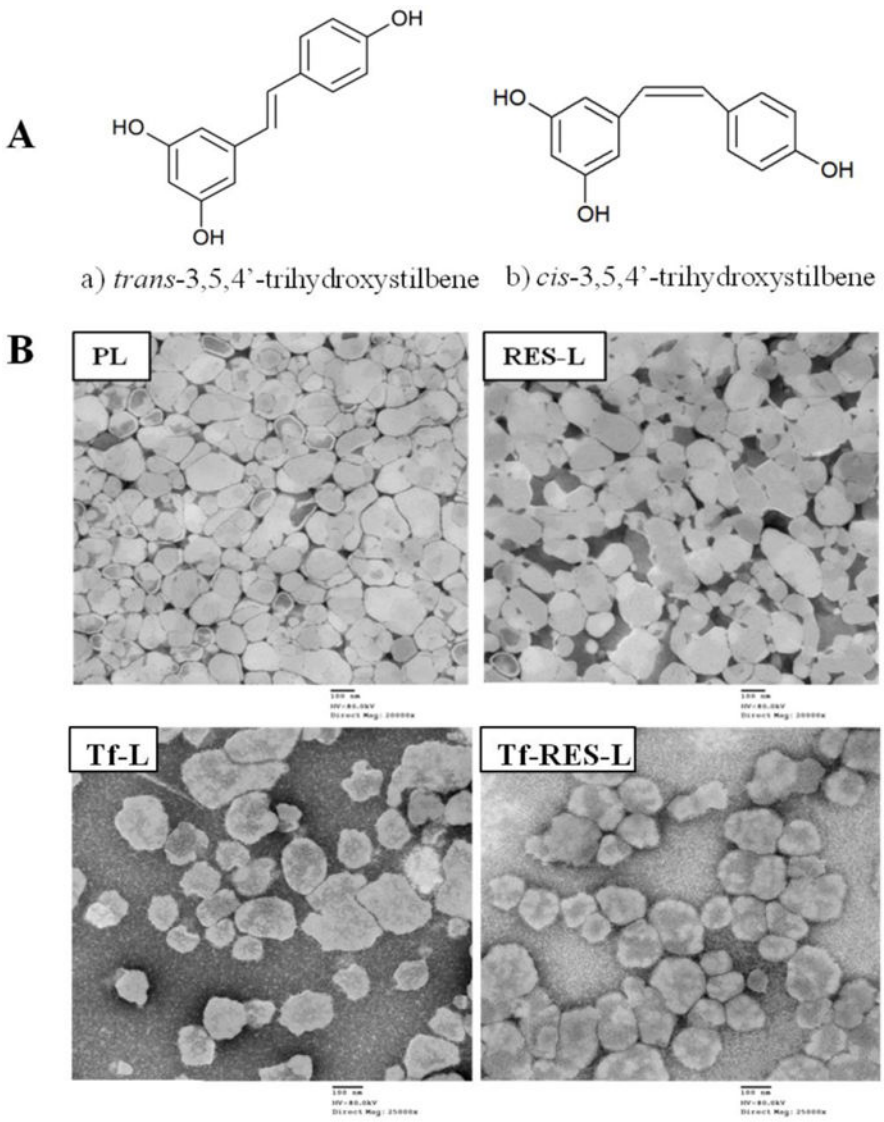

Figure 1. Chemical structure of resveratrol and TEM images

(A) Stereoisomers of resveratrol (a&b). The *trans* isomer is the biologically active form of the drug **(B)** Transmission electron microscopy (TEM) images of PL and RES-L at 20000X direct magnification and of Tf- L and Tf-RES-L at 25,000X direct magnification (Scale bar 100 nm).

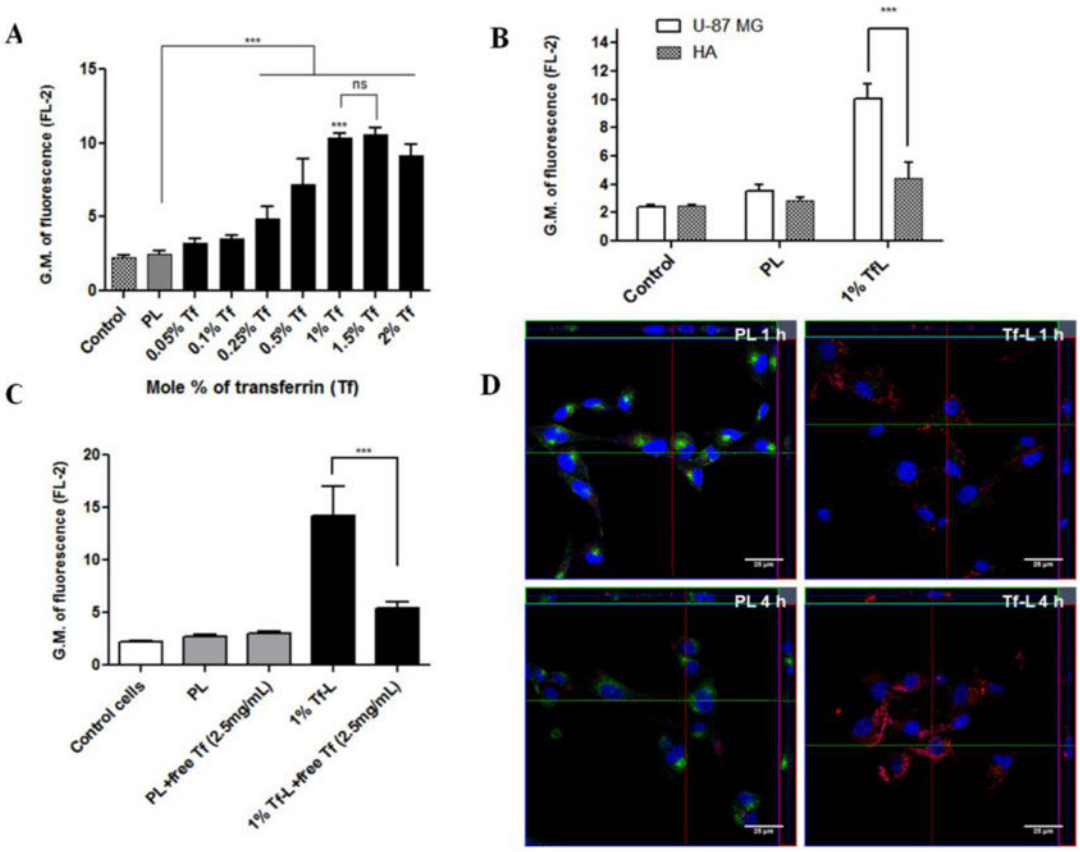

Figure 2. Cell association and internalization of Tf-L

(A) U-87 MG cells were treated with Rh- labeled Tf-L with varying Tf densities (0.05-2 mol %) on their surface for 4 h. **(B)** U-87 MG and HA were treated with Rh-labeled PL and 1%Tf-L for 4 h. **(C)** U-87 MG cells were treated with Rh-labeled Tf-L for 4 h either with or without pre-treatment with free Tf (2.5 mg/ml) for 30 min to study the competitive inhibition of Tf-L uptake. Data are plotted as geometric mean of fluorescence in the FL-2 channel (mean ±SD) from at least three independent observations. **(D)** U-87 MG cells were treated with Rh-labeled PL and 1% Tf-L at a final lipid concentration of 0.1 mg/ml for 1 h (top panel) or 4 h (bottom panel) respectively. Nucleus was stained with Hoechst 33342, and Tf-Alexa Fluor 680® was used as the endosomal marker. The cells were analyzed by confocal microscopy. Scale bar, 25 μm. Representative orthogonal projections of PL and Tf-L treated cells at 1 h and 4 h showing XY, YZ and XZ planes respectively. The main image shows the XY plane, the section to the right on the image represents the YZ plane and the section at the top of the image shows the XZ plane of the image.

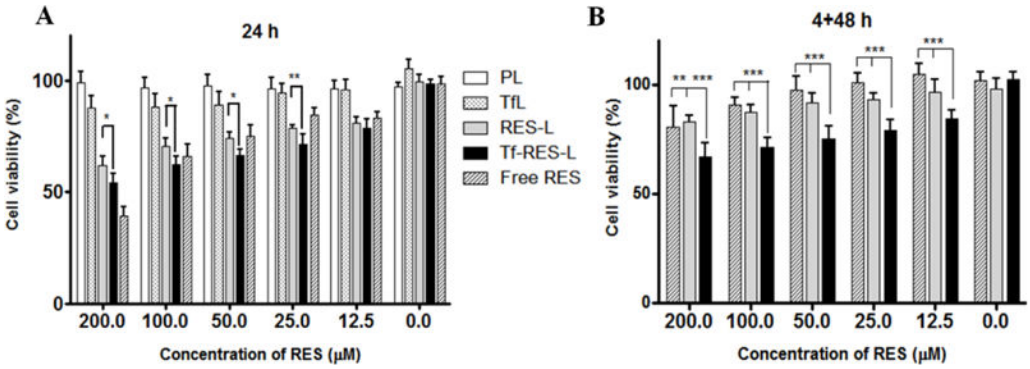

Figure 3. Cytotoxicity of RES formulations

(A) U-87 MG cells were treated with free RES, RES-L or Tf-RES-L continuously for 24 h or for **(B)** 4 h followed by a wash and an additional 48 h, before assessment of cytotoxicity. PL and Tf-L were used as controls. Cells were treated with formulations containing 12.5-200 μM RES. Data are plotted as mean ±SD, averaged from triplicate wells in at least 3 independent experiments. One-way ANOVA was used to compare between groups, $p < 0.05$ was considered significant (*p<0.05, **p < 0.01, ***p< 0.001).

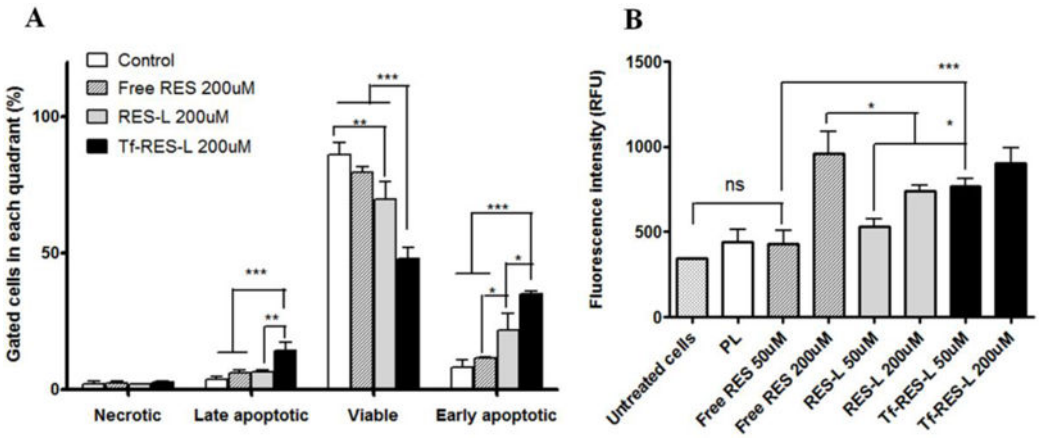

Figure 4. Apoptosis and caspase 3/7 activity in U-87 MG cells

(A) U-87 MG cells were treated with RES formulations for 24 h before staining with AnV-Alexa Fluor 488® and PI and analyzed by flow cytometry. Untreated cells served as controls. The fluorescence of PI was recorded in the FL-3 channel and that of AnV was recorded in the FL-1 channel. Cells labeled with one or both the compounds were analyzed using a quadrant plot. **(B)** U-87 MG cells were treated with formulations for 24 h. After removal of the drug containing media, caspase reagent was added to the cells. The fluorescence was read after 4 h. The fluorescent product generated was proportional to the amount of caspase-3/7 cleavage activity of the sample. Data are represented as mean ± SD, from three separate studies. One-way ANOVA was used to compare between groups, $p < 0.05$ was considered significant (* $p < 0.05$, ** $p < 0.01$, *** $p < 0.001$).

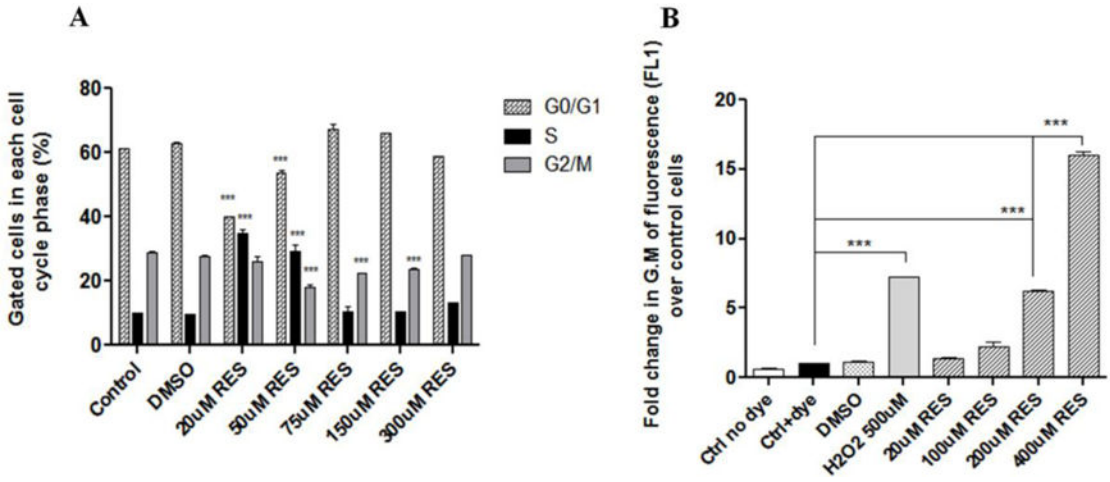

Figure 5. Effect of RES on cell cycle and ROS generation in U-87 MG cells

(A) Cells were treated with free RES in DMSO (0-300 μM) for 24 h. Following treatments, cells were collected and processed for cell-cycle analysis. All comparisons are with the control (untreated) cells. **(B)** Cells were treated with CM-H_2DCFDA (1 μM) for 30 min, followed by treatments for 1 h with free RES (20-400 μM) to study the generation of ROS. Following the 1 h incubation, cells were processed for flow cytometry. Results are represented as fold change in the geometric mean of fluorescence (FL-1) over control cells (B). Data are plotted as mean ±SD, averaged from triplicate wells in at least 3 independent experiments. One-way ANOVA was used to compare between groups, p <0.05 was considered significant (***p< 0.001).

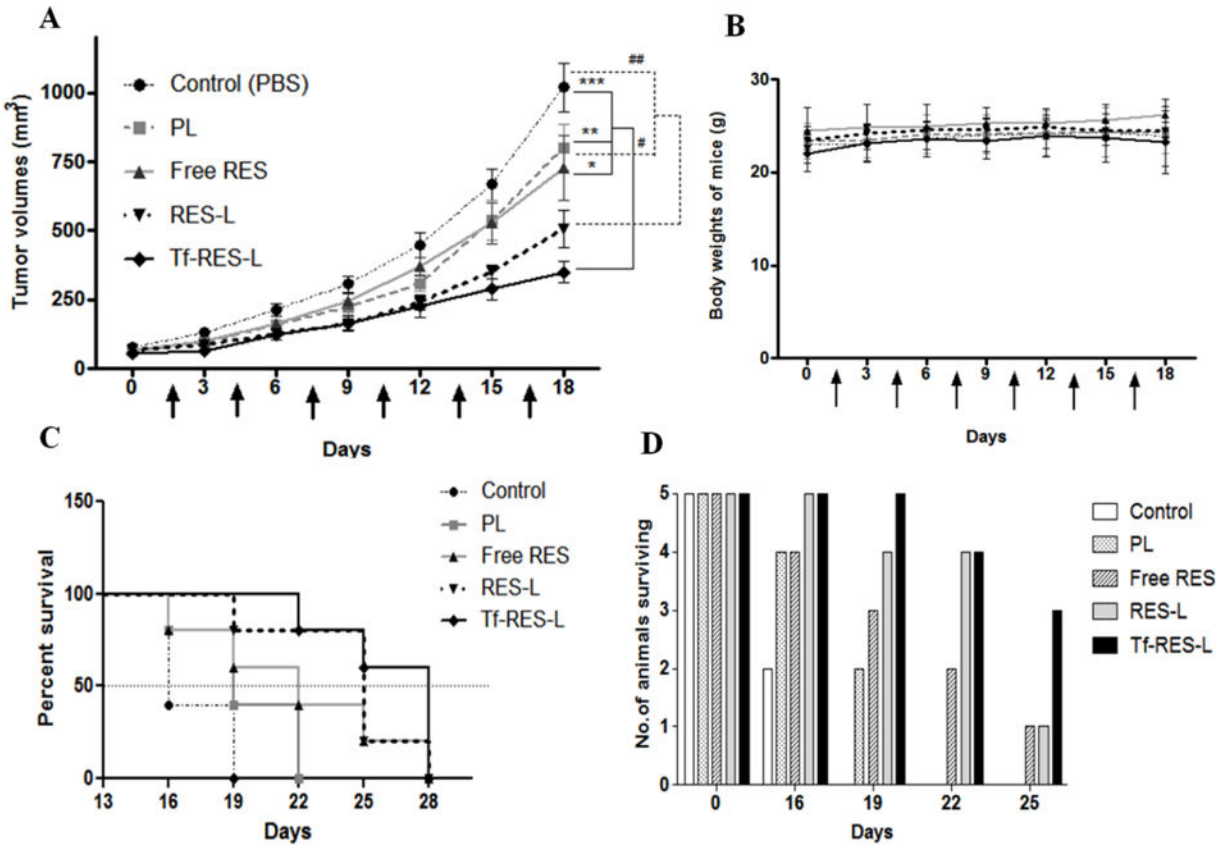

Figure 6. Effects of RES formulations on tumor growth inhibition and survival in U-87 MG tumor xenograft bearing mice

(A) The figure represents a line-graph for the tumor growth inhibition study. Arrows indicate the treatments, which were administered every third day. Statistical comparisons are shown at the end of the treatment period. The solid lines and * show comparison of the PBS, PL and free RES groups with the Tf-RES-L group, and the dashed lines and # show comparisons between the PBS and PL groups with the RES-L group. Tumor volumes are represented as Mean ± SEM for 5 animals per each treatment group. Two-tailed Student's t-tests were used to compare between treatment groups and $p < 0.05$ was considered statistically significant (* $p < 0.05$, ** $p < 0.01$and *** $p < 0.001$) **(B)** Body weights of mice recorded during the study. Data are represented as mean ± SD for each group of animals. **(C)** A modified survival analysis was carried out for all the mice that were included in the tumor-inhibition study (n=5 per group). The end point was a tumor volume of 1000 mm^3. Kaplan-Meier survival curves were plotted for each treatment group and the data were analyzed using the Log-rank (Mantel-Cox) test, $p < 0.05$ was considered significant. **(D)** Column graph of the number of animals surviving in each treatment group during a 25-day period.

Table 1

Characterization of liposomes

Lipid composition (molar ratios)	Liposomes	Particle diameter (nm ± S.D)	PDI	Zeta potential (mv ± S.E)	% Drug loaded
EggPC:Chol:DSPE- PEG2000- CHEMS:DOPE (61:24:3:6:6)	PL	180.5 ± 5.8	0.11	−39.4 ± 1.3	
	RES-L (3%w/w RES)	182.3 ± 12.1	0.11	−41.7 ± 1.6	70−75%
	Tf-L (1 mol% Tf)	200.2 ± 2.4	0.11	−35.0 ± 1.5	
	Tf-RES-L (1 mol% Tf, 3%w/w RES)	211.2 ±0.8	0.09	−34.1 ±0.9	70−75%